APPLICATION OF MODIFIED HOEK-BROWN TRANSITION
RELATIONSHIPS FOR ASSESSING STRENGTH AND POST YIELD
BEHAVIOUR AT BOTH ENDS OF THE ROCK COMPETENCE SCALE

Trevor G. Carter, PhD, PEng.
Rock Mechanics Group, Golder Associates, Toronto, Canada
Mark S. Diederichs, PhD, PEng.
GeoEngineering Centre, Queen's University, Kingston, Ontario, Canada
José L. Carvalho, PhD, PEng.
Rock Mechanics Group, Golder Associates, Toronto, Canada

ABSTRACT

Support system design for tunnels and underground excavations has for many years relied heavily on the use of rock mass classification systems and the Hoek-Brown failure criterion as a means for characterizing rockmass behaviour. Because of their development, both the GSI system and the Hoek-Brown criterion admirably characterize most "normal" rockmasses from the viewpoint of their behaviour for rock excavations. They however run into difficulties when applied at the two ends of the rock competence scale. This is largely because block size and incipient strength is such that rockmass behaviour in these domains tends not to be controlled by interblock shear strength but rather by material strength. At the low end of the rock competence scale (UCSi ? 15 MPa and GSI generally <30) discontinuities play less of a role and rock mass strength tends to matrix strength. Similarly, at the high end of the scale (GSI$\cong$65, $m_i\cong$15), because discontinuities are now widely spaced, block size becomes so significant that again, intact material behaviour rather than the fracturing becomes the dominant factor controlling rockmass strength.

In this paper several case examples are presented to illustrate the application of the high-end (spalling) and low-end (weak ground) transition Hoek-Brown relationships proposed by Carter, Diederichs and Carvalho, (2007) as a basis for better defining rock mass behaviour at the extreme ends of the rock competence scale.

1.0   INTRODUCTION

Support design for mining or civil purposes relies heavily on use of rockmass classification procedures, not just as a tool for empirical support assessment but also for characterizing rockmass strength. However, for many deep mines and deep tunnels where high stress states can be problematic, it frequently becomes quite difficult to accurately characterize rock mass strength and develop appropriate support designs through the use of conventional rock mass classification based support charts or through application of the generalized Hoek-Brown criteria relationships, (as originally introduced in 1980, with various updates through to Hoek et al., 2002). In general, characterizing rockmass strength through use of the Hoek-Brown relationships as the

basis for design of support systems is fundamentally based on the principle that structure within a rockmass acts to reduce both the cohesion and frictional properties, represented by downgrading "*s*" and "*m*" respectively in the Hoek-Brown criterion.

Within rock mass classification systems the premise is also made that structure exerts most control on rock mass behaviour, and hence worst case classification parameter values and overall lowest rockmass strengths are typically associated with the most heavily fractured rockmasses. Although the four most commonly used classification systems, RMR, Q, RMi and GSI, (Bieniawski, 1973, 1976, Barton et al., 1974 & Barton, 1976, Palmström, 1995 and Marinos & Hoek, 2000) have some input parameter relationships that directly or indirectly reflect intact rock strength, the importance given to rock strength in all of these classifications is generally limited. For the mid-range of the rockmass competency scale, where block size and incipient strength is such that rockmass behaviour tends to be controlled by inter-block shear strength rather than by material strength, the empirical Q-system and Mathews-Potvin type support design charts (Grimstad & Barton, 1993, Potvin et al, 1989) and most numerical modelling tools function well. However, towards the two ends of the rock competence scale (ie., for very low strength rocks and also, for spall-prone, high GSI rockmasses) difficulties can be experienced in not only properly classifying such rockmasses, but also in application of the Hoek-Brown criterion for determining rockmass strength.
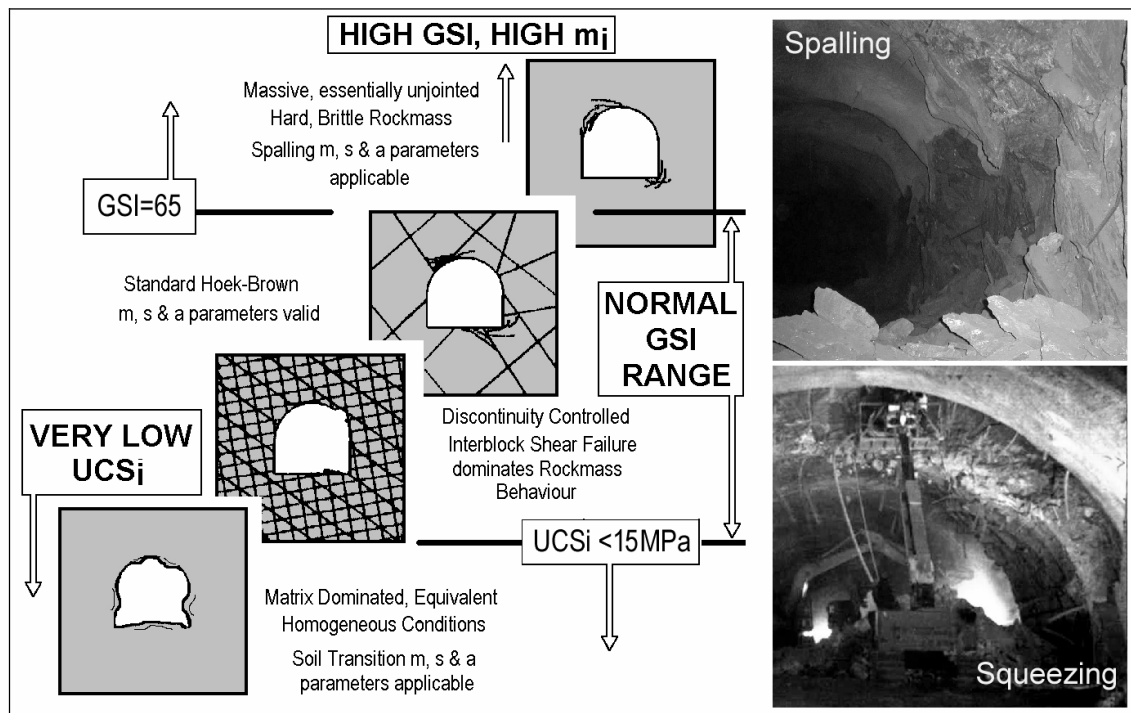

Figure 1: Transition from standard GSI and Hoek-Brown *m*, *s* and *a* parameter applicability to proposed transitions – between (***top right***) high GSI, high m_i spall-prone rockmasses ($m_i \cong 15$ and GSI $\cong 65$), subject to brittle spalling and strainbursting failure behaviour and (***lower left***) very low strength rocks (UCSi = σ_{ci} < 10–15MPa), subject to shear failure and squeezing behaviour (ref. also lower photo, courtesy E. Hoek).

This difficulty arises, largely because outside this "normal" mid-range of rockmass competence, behaviour becomes less discontinuity controlled, (Figure 1). At the low

end of the scale (for very weak rocks with UCSi < 10–15MPa) rock mass strength conforms to matrix strength and structure has minimal impact. Similarly, at the high end of the rock competence scale (GSI $\cong$ 65 and $m_i \cong 15$) in situ rock mass strength for a given rock type again is controlled by material strength, reaching a maximum strength consistent with spontaneous crack propagation (spalling) after crack initiation for rocks with high m_i values and with crack accumulation, interaction and coalescence (resulting in matrix shearing) for high GSI rocks with low or moderate m_i values.

2.0 EXTENDED HOEK-BROWN PARAMETER APPLICABILITY

This paper builds on three recent publications (Carter et al., 2007, Carvalho et al., 2007 and Diederichs et al., 2007) that address the fact that at both ends of the rock mass competence scale current classification-based strength criteria face limitations in characterizing a rockmass in a way that is consistent with its behaviour.

2.1 Transition Relationships

The nature of the two proposed transitions that bound the range of typical rockmass behaviour through the normally encountered mid-range of rock block size conditions, (30<GSI>70) approximately, differ markedly. At the low end of the rock competency scale, (when UCSi<15MPa), the transition from interblock shear failure (which is well modelled by the Hoek-Brown failure criterion and the GSI system) downwards as rock mass behaviour becomes more matrix controlled, is quite gradual, as illustrated in the left plot on Figure 2; as compared to the transition at the high GSI end of the scale, which is quite abrupt and variable depending on m_i. This variability reflects in large part the major changes in material behaviour occurring at the upper end transition as shown in the right hand diagram on Figure 2.
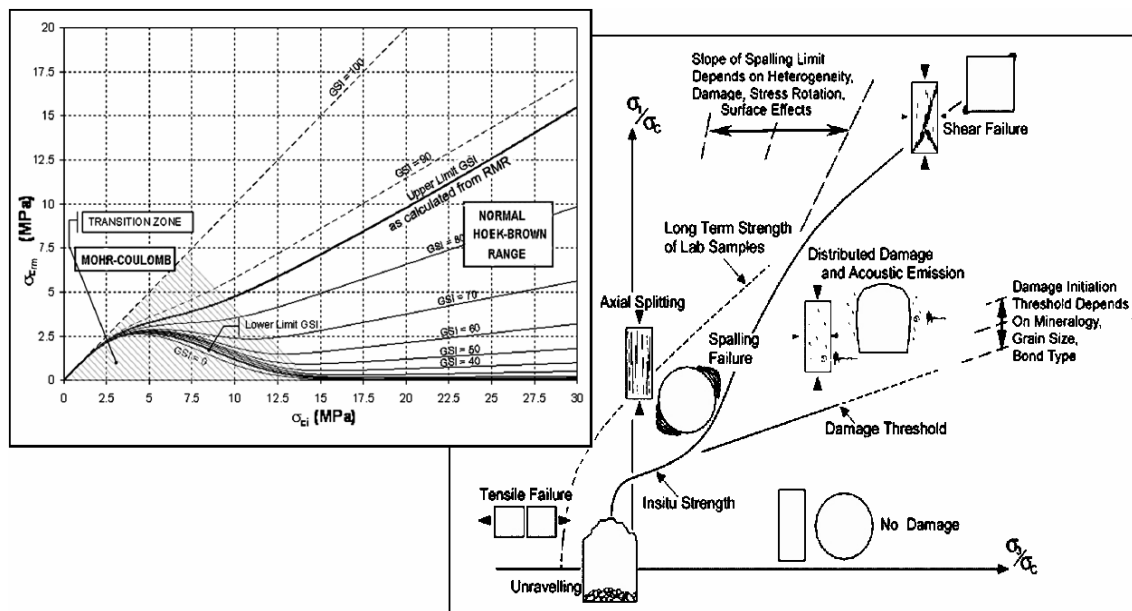

Figure 2: Transition Behaviour – *Left diagram = Low-End Soil–Rock Transition* with rockmass strength, UCS$_{rm}$ = σ_{crm} plotted with respect to intact UCSi = σ_{ci} and GSI, (from Carvalho et al., 2007) – and *Right diagram = High-End Behaviour* showing damage initiation and propagation limits for spalling in high GSI, spall-prone rockmasses with strength reduction

insitu from the long term lab strength (crack coalescence) to the damage initiation threshold (from Diederichs, 2003).

This difference in behaviour between the two transitions is clearly evident when the two relationships are plotted alongside each other with reference to the Hoek-Brown "normal" behaviour response. As illustrated in Figure 3, which plots normalized rockmass strength against GSI, the low strength transition curves (which are plotted as dashed lines across the graph and which re-plot the curves from the left hand diagram on Figure 2) fan out fairly uniformly from the Hoek-Brown conventional GSI curve to the Mohr-Coulomb line (across the top of the chart) suggesting a fairly smooth transition in behaviour. The curves show the appreciable rockmass strength gain predicted to develop with decreasing intact matrix strength as compared with the conventional Hoek-Brown inferred strength.
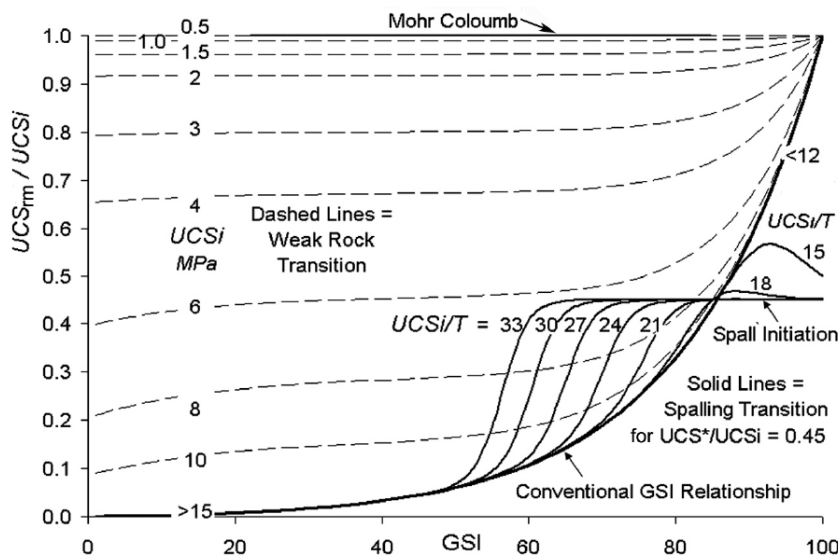

Figure 3: Normalised Rockmass Strength (UCS$_{rm}$/UCSi) as a function of Rock Quality (GSI) illustrating marked differences between conventional Hoek-Brown behaviour and transition functions. (Spall transition threshold set at typical value, UCS*=0.45UCSi)

The form of the relationships for the more abrupt upper transition, particularly for high m_i rockmasses (ie., for $m_i \approx \sigma_{ci}/\sigma_t$ = UCSi/T >15) is much more complex. As shown by the curves on the right side of Figure 3, this upper end spalling transition predicts significantly lower rockmass strengths for essentially intact insitu rock masses with moderate to high m_i values at high GSI, than suggested by application of the conventional Hoek-Brown – GSI relationships. In this, the upper end transition function replicates fairly faithfully observations from deep mining and tunnelling situations where a large body of evidence suggests that application of the Hoek-Brown criterion routinely overestimates rockmass strength. The curves on Figure 3 also illustrate another frequently noted observation that for moderately jointed rock with GSI values as low as 55 but with very high m_i values (ie., mostly for rocks that are brittle in nature and principally in the class of so-called hard rocks (granites, norites, crystalline limestone, gneisses, quartzites, etc), much higher rockmass strengths are suggested than would be predicted using the conventional Hoek-Brown – GSI relationships.

3.0   LOW-END TRANSITION

In order to develop the low-end transition function two basic bounding limit assumptions have made on the basis of available laboratory data and numerical modelling evaluations (as discussed in Carvalho et al, 2007). These bounding limits, which are clearly shown on Figure 3, are (i) that material behaves as a "normal" Hoek-Brown rockmass at intact matrix strengths of greater than about 15MPa and (ii) that UCSi = σ_{ci} = 0.5MPa can be considered a practical upper "soil strength" limit, below which it is difficult for physically meaningful structural discontinuities to exist. Between these limits, up to of the order of 10-15 MPa intact strength, after which structural features are discrete and dominant, there is increasing control due to remnant structure. Given these limits, and as discussed by Carvalho et al., 2007 because the more soil-like the material the more it tends to linear strength behaviour (a→1) compared to a much more non-linear strength envelope for rock, the low-end transition expression has been developed to fit these criteria with the following form:

$$f_T(\sigma_{ci}) = \begin{cases} 1 & , \quad UCSi \le 5p_a \\ e^{\frac{-(UCSi - 5p_a)^2}{250p_a}} & , \quad UCSi > 5p_a \end{cases} \qquad (1)$$

where p_a is atmospheric pressure. (It should be noted (i) that the numerator in the exponent term in this transition function was erroneously reported in Carvalho et al., 2007 and in Carter et al., 2007 as GSI instead of UCSi; and (ii) that the transition function limits are expressed in terms of atmospheric pressure so that the function is independent of the unit system. Because most practitioners work with rock mass strengths in MPa, this relationship has been dimensionalized in Table 2 (presented subsequently). Incorporating this transition relationship into the Hoek-Brown criterion is simply accomplished, as follows:

$$s^* = s + (1-s)f_T(\sigma_{ci}) \qquad (2)$$

$$a^* = a + (1-a)f_T(\sigma_{ci}) \qquad (3)$$

$$m_b^* = [m_b + (m_i - m_b)f_T(\sigma_{ci})]/(4a^* - 1) \qquad (4)$$

In the above expressions the parameter m_b* in the linearized form of the envelope is a more complex expression due to the adjustment made from the original Hoek-Brown formulation in order to maintain the ⅓ m_i relationship obtained by classical Hoek-Brown fitting with the exponent a = 0.5.

4.0   HIGH-END TRANSITION

4.1   Damage Initiation and Hard Rock Strength

For hard rock materials, extensile cracking rather than shear is the primary form of damage, even under compression, (Stacey 1981; Tapponier & Brace 1976; and Griffith 1921, for example). Under low confinement, the propagation of extensile cracks leads to spalling, such as observed at depth around hard rock openings of high rockmass quality in the immediate vicinity of an excavation boundary. This mechanism is predominantly tensile in nature, and thus differs markedly from more "normal" shear behaviour assumed throughout the rest of the GSI range.

4.2   Hard Rock Lower and Upper Bound Strength

Lower bound in situ compressive strength for excavations in hard rocks corresponds to an extension crack damage initiation threshold that is a function of the nature and density of internal flaws and heterogeneity. Numerous researchers (Pelli et al. 1991, Martin et al. 1999, Brace et al. 1966, Wagner 1987 and Castro et al. 1996) have shown that failure in massive hard rock excavations, begins when the tangential stress limit at the excavation boundary exceeds 33% to 50% of the rock's intact UCSi. This threshold (UCS*) when expressed relative to laboratory Unconfined Compressive Strength (UCSi) can be as low as 1/3 for igneous rocks (Lajtai & Dzik, 1996) and as high as 1/2 for dense clastics, (Pestman & Van Munster, 1996).

The mechanisms illustrated in the diagrams in the lower left part of Figure 4 can occur even at moderate confining stresses, but they can only propagate under conditions of locally low confinement. At high confinements crack accumulation (recorded as acoustic emissions or microseismic events) must occur before crack coalescence can lead to propagation. In this case the upper bound yield strength insitu corresponds to the long term strength of laboratory samples (ref. left hand dashed curve in the right hand diagram on Figure 2).
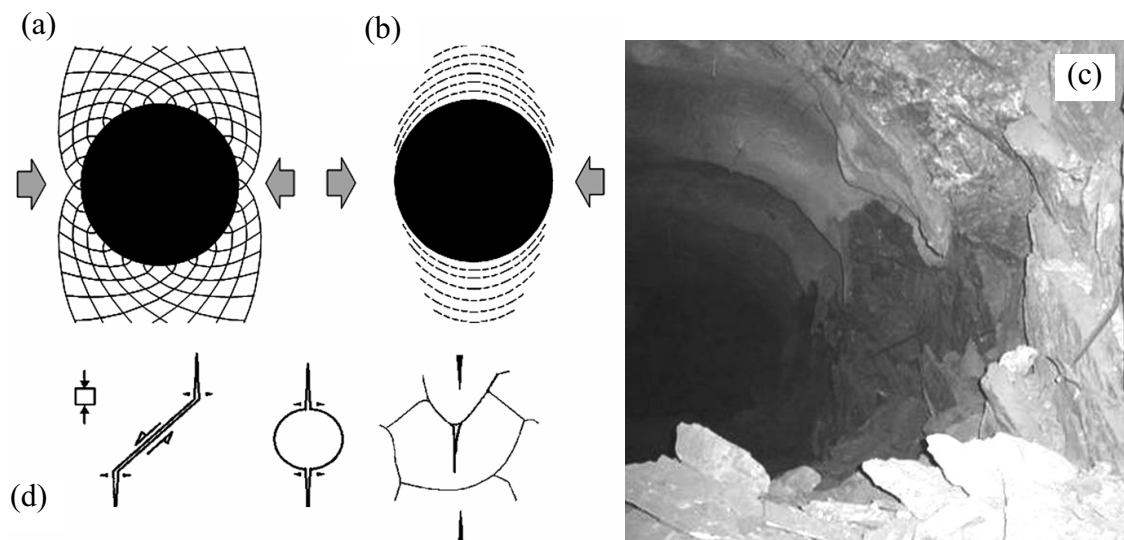

Figure 4:   (clockwise from top-left) (a) Shear failure around a tunnel; (b) spalling damage in hard rocks at high GSI; (c) example of brittle spalling and strainbursting in a deep mine opening; and (d) mechanisms of crack initiation in hard rock.

At low confining stress near an excavation boundary however, spontaneous propagation of initiating extension cracks is possible. In this case the yield strength insitu collapses to the damage initiation threshold line as shown in the lower right hand part of the right hand diagram on Figure 2.

4.3   Hard Rock Strength Using Hoek-Brown Empirical Criteria

In order to apply the Hoek-Brown criterion in its generalised non-linear form for rockmasses with GSI $\cong$ 65 again a different approach needs to be taken for parameter definition than just the normal GSI and UCSi determination, and consideration needs to be given to spalling processes and tensile cracking behaviour. As outlined by

Diederichs et al., 2007, definition of spalling behaviour for modelling in an inelastic Hoek-Brown formulation can be readily achieved by carrying through the following steps with reference to Figure 5:

(i)   Determine UCS*, the onset of "systematic cracking" (B in Figure 5), from acoustic emission or radial strain data,

(ii) Obtain a reliable estimate of tensile strength, T (eg., from carefully executed Brazilian testing with close inspection during and after testing to ensure correct end bearing and clean initiation of a medial fracture),

(iii) Set $a_{SP} = 0.25$ (ie., assuming "peak" conditions – spalling initiation), …and…

(iv) knowing the basic laboratory unconfined compressive strength (USCi) for the rock material, calculate appropriate values of s_{SP} and m_{SP} from:

$$s_{SP} = \left(UCS*/UCSi\right)^{1/a_{SP}} \qquad (5)$$

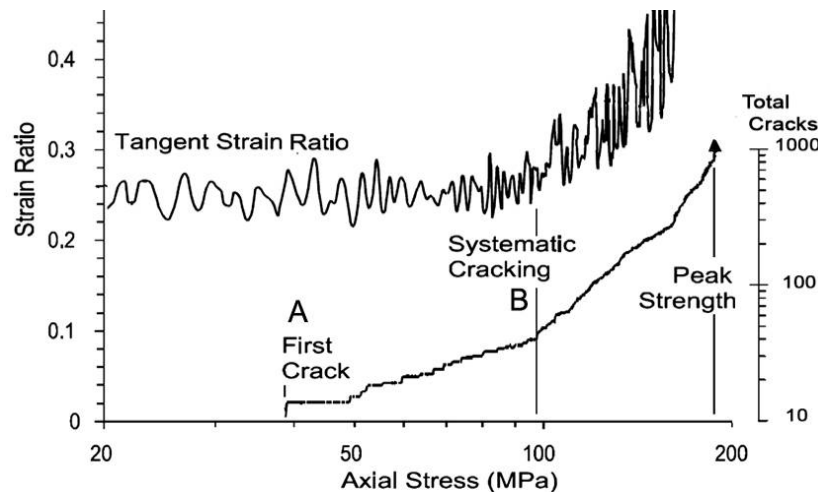$$m_{SP} = s_{SP}\left(UCSi/|T|\right) \qquad (6)$$

Figure 5: Determination of damage initiation thresholds for rock under compressive loading using strain and acoustic emissions (after Diederichs et al., 2004).

Note that these parameters apply only for the onset of systematic cracking and thus they define the "peak" or spalling initiation threshold curve (as shown by the lower slope gradient curve on Figure 6).
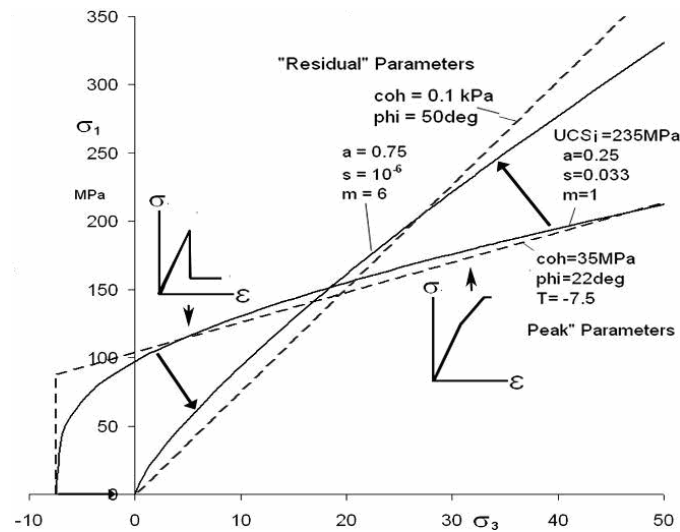
Figure 6: Example of "peak" and small strain "residual" strength parameters for damage initiation and spalling limits (Diederichs 2007).

However, as initiating spall cracks can only propagate under low confinement a second limit (defined here as the "residual" state) is therefore needed, defining the condition constraining spalling behaviour. Based on the experimental work of Hoek (1968) and on numerical simulations described by Diederichs (2007) a limit can be postulated to create a transition between spalling behaviour at low confinement, controlled by the initiation threshold, and a shear strength closer to the long term strength limit for the intact rock (as extensile crack propagation is suppressed) at higher confinements. This, the "residual" spalling limit can be approximated using $a_{SP} = 0.75$, $s_{SP} = 0$ and a residual m_{res} value of approximately $m_i/3$ (typically 5-10).

Substituting these spalling parameter values into the generalized non-linear Hoek-Brown formulation results in the two curves shown on Figure 6 Equivalent Mohr-Coulomb thresholds, as also shown in Figure 6 can also be defined, with the "peak" parameter Mohr-Coulomb envelope line defining the damage initiation threshold and the "residual" parameter envelope line defining the spalling confinement limit.

As might be expected, the shape of the "residual" limit curve is very sensitive to confinement, as provided by natural interleaving of spalled material, by rock reinforcement or by any other constraint method. Determining the absolute magnitude of applicable constraint in any given situation is not always straightforward, but some measure of natural or applied constraint degree can however be achieved through use of the Hoek-Brown dilation parameter, D in the generalized relationships (Hoek et al., 2002). For unrestrained fallout or for loose retention (ie., simulating minimal feedback pressure against unyielded rock), dilation should be set to zero. For light support (mesh, spot bolts etc), dilation can be set according to an appropriate non-associative flow rule substituting m_{dil} for m_b using an appropriate value of $m_{dil} \approx m_{res}/(8 \text{ to } 10)$ consistent with Ryder & Jager (2002), and Vermeer & de Borst (1984) where m_{res} is the value specified in the yield function for "residual strength" (ie., approximately $m_i/3$, consistent with $a_{SP} = 0.75$).

Unfortunately, such constant dilation flow rules in many codes present difficulties with convergence in brittle modelling. A practical alternative is therefore to model the depth

of failure with no dilation (ie., assuming minimal retention/support) or with the dilation parameters as specified above where moderate support pressure is assumed. Once the failure depth is determined, a better approximation of likely displacements can then be obtained from the depth of failure and the empirical support-dependent bulking factor, B.F. relationship, simplified from Kaiser et al (1995), viz

$$\text{Inelastic radial displacement} = G \times DOF \times B.F., \quad \text{where} \quad B.F. = 0.3e^{\left(\frac{-P}{70}\right)} \quad \text{(7 \& 8)}$$

… and where *P* is the applied support pressure in kPa, *DOF* is the depth of failure and the factor *G* accounts for a gradient of dilation from the wall to the edge of the yielding zone; which, for a linear assumption, can be specified with G=0.5.

In using this approach for evaluating the extent of likely inelastic radial displacement it is important to look at plastic shear strain gradients within the "yielded" rockmass to determine if the rock is actually failing or merely damaged. The region enclosed by significantly elevated plastic strain contours should be considered as spalling, while apparently yielded regions with very low relative strain values would more likely correspond to stress paths above the damage threshold but below the spalling limit. Note: only rock depth with significantly elevated shear strain should be considered.

4.4   Transition Between Conventional Behaviour and Spalling

The transition from conventional Hoek-Brown shear behaviour to spalling behaviour, as proposed by Diederichs et al., 2007 considers rockmass quality, (as indicated by GSI), and the ratio between compressive strength and tensile strength (as estimated by the Hoek-Brown parameter m_i) and takes the following form:

$$X_{TRANS} = X_{GSI} + (X_{GSI} - X_{SP}) f_{SP} \quad \text{(9)}$$

where

$$f_{SP} = \frac{1}{1 + e^{\left(100\left[2 + \frac{D}{5} - \left(\frac{GSI}{60}\right)^{1/3} - \left(\frac{UCSi}{34T}\right)^{1/5}\right]\right)}}$$

… and where the X's represent the values of *a, s* and *m*, according to their subscripts, for conventional *"GSI"* assessment (as per Hoek et al., 2002) and *"SP"* corresponds to their values for spalling assessment, both for "peak" and "residual" conditions.

Application limits are specified discretely in Table 1 below or for most practical cases can be estimated from the plot of the transition function as presented in Figure 3.

Strength Ratio UCSi/T	GSI <55	GSI 55 to 65	GSI 65 to 80	GSI >80
<8	GSI	GSI	GSI	GSI
9 to 15	GSI	GSI	GSI	GSI/SP
15 to 20	GSI	GSI/SP	SP/GSI	SP
>20	GSI	GSI/SP	SP	SP

Table 1: Application ranges for Spalling (SP) and conventional GSI approach

5.0   CASE EXAMPLES – HIGH GSI ROCK MASSES

To illustrate the application of these types of analyses assuming hard rock spalling parameters and using currently available computer modelling codes, several examples from mining and deep tunnelling situations have been chosen, as follows:

5.1   AECL-URL Tunnel in Massive Granodiorite.

For this case (Figure 7) the Hoek-Brown spalling parameters, summarized in Figure 6, were used to simulate the breakout observed in the URL test tunnel (Martin, 1997). In order to indirectly model the influence of moderate support (retention) versus no support, use was made of the dilation parameter as a constraint approach.
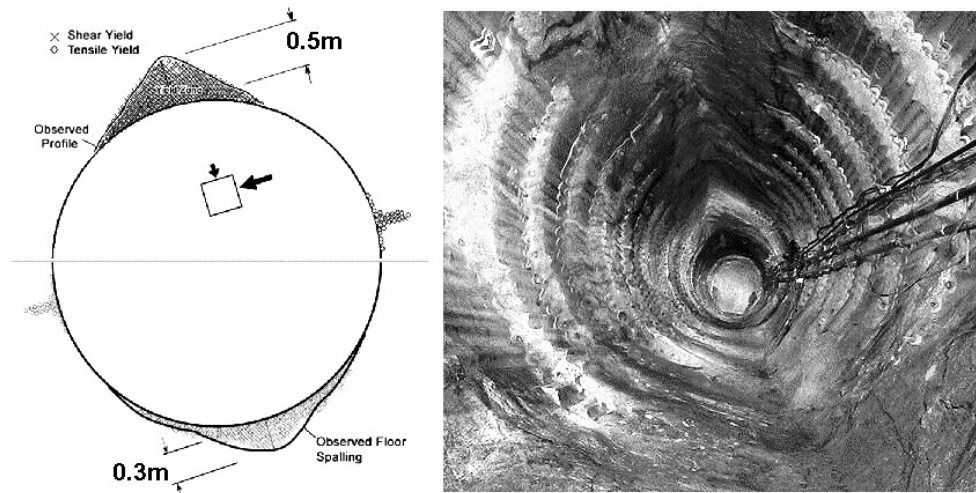
Figure 7: Example of non-linear modelling of URL Test Tunnel.

Figure 7 illustrates, on the left, the results of the spalling simulation analyses compared with the observed conditions. The roof (modelled without dilation) was essentially unsupported while the floor was constrained under aggregate fill (modelled with dilation, $D = m_{res}/8$ to simulate feedback confinement due to the retained material). In both the floor and the roof cases, the modelled failure depth and angular extent is accurately simulated. As a second comparison, for the same case record, the equivalent Mohr Coulomb parameters derived from Figure 6 were used in FLAC3D to simulate the tunnel but in this case without dilation, but with a transition based on the plastic shear strain parameter relationships shown on the left of Figure 8.
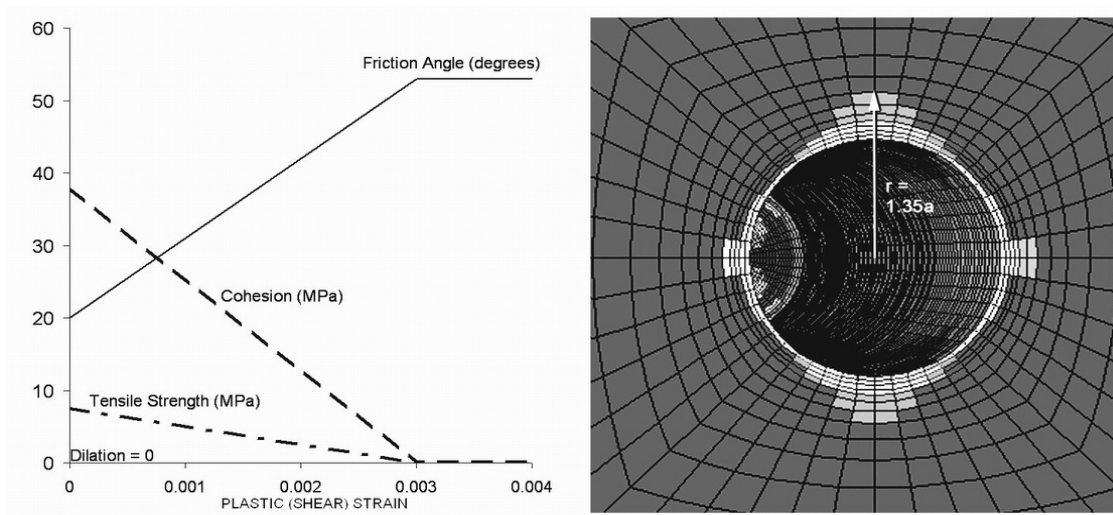
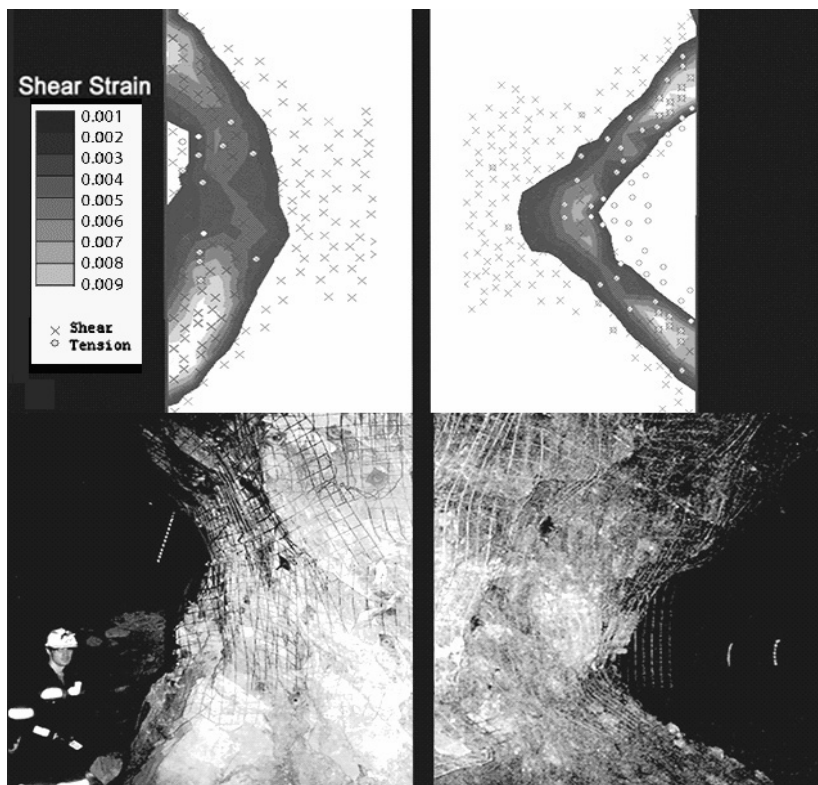Figure 8: Application of equivalent Mohr-Coulomb parameters in FLAC3D

Figure 9: Pillars (McCreedy Mine) modelled using spalling Hoek-Brown (*left*) and equivalent Mohr-Coulomb (*right*) parameters. Both models capture observed behaviour.

5.2   Hard Rock Mine Pillars – McCreedy East Mine, Sudbury

The choice of Mohr-Coulomb or generalized Hoek-Brown parameters to simulate progressive failure (Figure 6, Figure 9) is one of preference. Both produce acceptable results in most situations, but with the Mohr-Coulomb approach tending to better reproduce expected tensile behaviour for rectangular openings while the Hoek-Brown

approach tends to produce less spurious and more reliable results for circular geometries, where tension is not such a major factor.

Figure 9 illustrates a simulation of pillar failure at McCreedy East Mine in Sudbury using equivalent Hoek-Brown and Mohr-Coulomb parameters. The overall failure (extent and initiation with respect to depth) is similar in both simulations although the geometry and dominant mode of rupture differs. In the Mohr-Coulomb analysis (top right) the non-dilatant and low-strain region bounded by a zone of high plastic strain, typical of square openings is well indicated. The failure mechanism observed in the field is a combination of extensional spalling (initiating away from the wall boundary) and dilatant shear in the corners. Such a resultant arch and relatively undisturbed roof or wall mass partitioned by the failing zone is commonly encountered in non-circular openings and was termed "baggage" by Kaiser et al (1995), due to its influence as non-bulking dead weight. Both behaviours reflected in the analysis can be found in the same rockmass in the same stress and geometrical environment, as shown by the examples.

5.3   Nathpa Jhakri Project, India

As part of the construction works for the 1500MW Nathpa Jhakri hydropower scheme through the Himalayas of Northern India, excavation was required of significant stretches of the 10.5m diameter Headrace Tunnel at depths well in excess of 1000m, (Hoek, 2001, Carter et al., 2005, Kumar and Dhawan, 1999). As explained in some detail in Carter et al., 2005, much of the tunnelling was through very variable geology, with some zones of highly silicified gneiss that exhibited face spalling and typical strain burst behaviour both during and subsequent to excavation.

In one of these tunnel sections, severe slabbing of the sidewalls and breakout of the crown and haunches developed some 50-60m behind the face, with multiple strain release events occurring soon after face blasting. In this zone approximately 400 resin and cement grouted rockbolts lost their heads and faceplates due to the significant slabbing and onion-skin spalling of 50-100mm thick slabs that developed mainly in the right haunch (Figure 10). As originally installed, (see inset photo) the grouted bolts were placed at 1.5m spacing longitudinally and transversely across the tunnel drivage, giving a nominal support pressure of approximately 50kPa.

Two sections of this breakout have been chosen for analysis here: a section in a more competent gneiss unit with UCS = 160MPa, (m_i=28) and GSI approximately 65 and a section with more intense foliation and a lower intact strength (UCS=110 MPa). The depths exceed 1300m but a combination of high tectonic stress, topography and fault occurrence results in a maximum stress of approximately 55 to 60 MPa inclined at 25 degrees from the horizontal with 20 to 25 MPa as the minimum orthogonal stress.

The non-linear spalling Hoek-Brown approach was applied first for the more competent rockmass, as shown in the principal stress plot in the top left of Figure 10. As is evident from the cross-section in the lower left of the figure, the right haunch shows significant shear strain (which indicates active yielding as opposed to distributed damage). Using Equation 8 with the depth of yielding indicated by the plastic strain contours a maximum bulking factor of 15% is estimated for the right haunch. Assuming

a linear bulking gradient in Equation 7, this translates to a wall displacement of approximately 10cm distributed over 1.3m, well sufficient to snap stiff rebar.
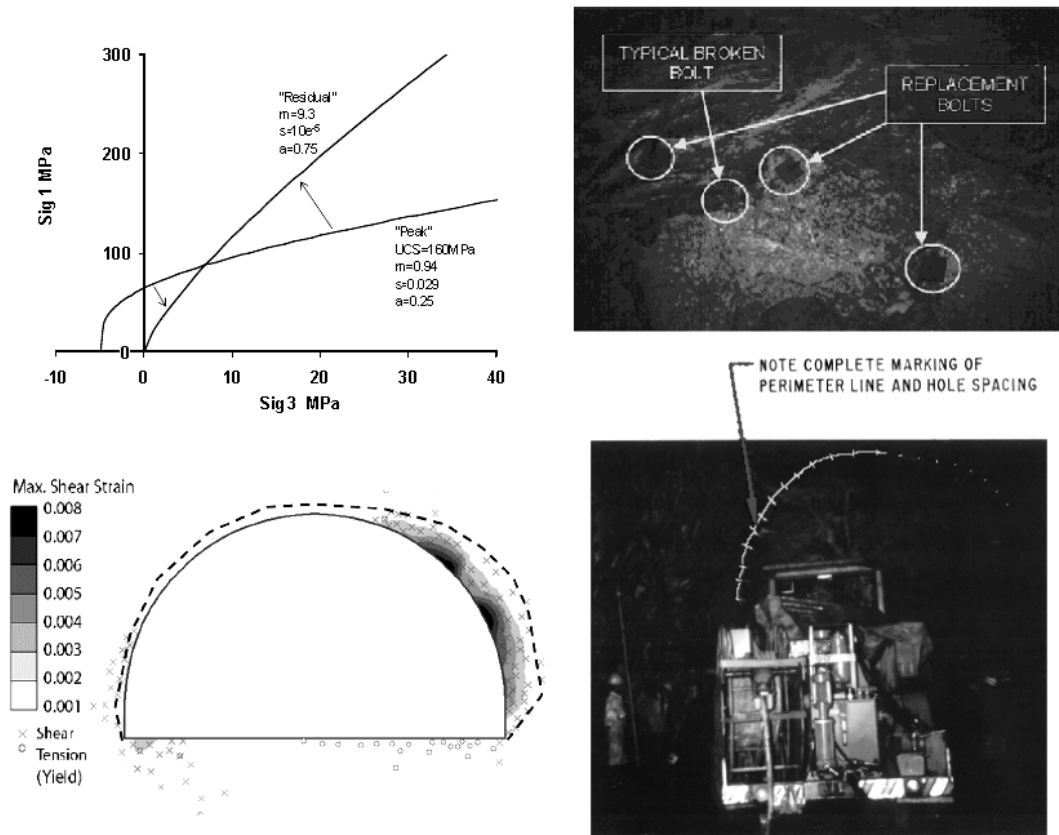

Figure 10: (***top left***) Spalling parameters for Nathpa Jhakri Nugalsari tunnel section (in good quality gneiss) with (***bottom left***) analysis results showing yield indicators and shear strain contours. Dashed line indicates surveyed breakout profile while top photo on right shows – broken & replaced bolts, and lower photo shows – initially well drilled blast profile.

A little further along the same segment of the Headrace, the tunnel encountered a more foliated, somewhat lower quality rockmass, with GSI's of 50 to 60 and a weaker intact strength (UCS=110MPa). As shown on Figure 11, for this tunnel segment the foliation also created an anisotropic stress distribution which also influenced the spalling process. For this reason the foliation here was treated separately by modelling it as discrete weakness planes (joint elements) and using a higher GSI estimate for the remainder of the rockmass (so as not to penalize the rockmass twice for the foliation).

Following the process described earlier, estimates were made of small strain "peak" and "residual" equivalent Mohr-Coulomb c, ϕ parameters for modelling this case, with the result shown in Figure 11, left plot. As is evident from the photograph of the notch breakout and the actual surveyed tunnel overbreak profile, the observed failure geometry is recreated faithfully. The fact that no breakout occurred on the opposite sidewall is of note, but explainable when displacements are calculated, which suggests that support on the lower left corner was sufficient to withstand the spalling and shearing processes.
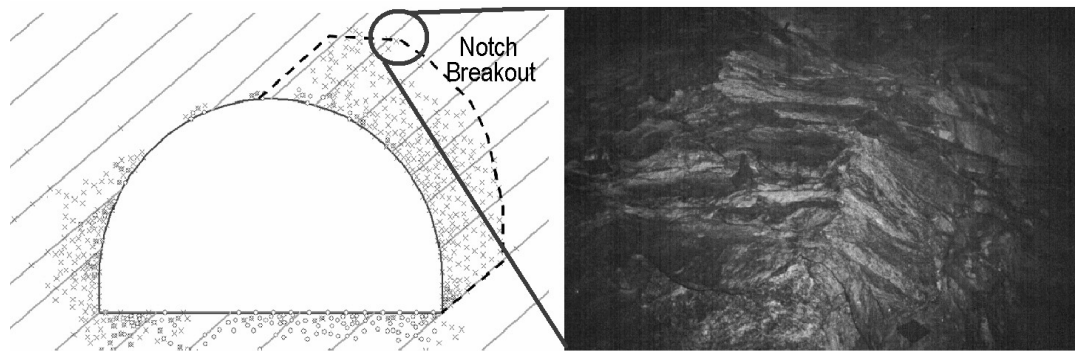
Figure 11: Spalling analysis for lower quality foliated rock. Straight lines indicate joint elements (foliation partings) and thick dashed line indicates observed breakout, with photo illustrating the deepest notch area at the centre of the right haunch breakout zone.

6.0   CASE EXAMPLES - WEAK ROCK

For weak rock the low-end transition function (as discussed earlier) is currently less well defined physically by laboratory and field data than the high-end transition relationships, being essentially a transfer function apportioning control of rockmass behaviour between the intact material (at the soil end of the competency scale) and the joint fabric (at the rock end of the transition). This is specified to occur over a range of uniaxial compressive strength, UCSi = σ_{ci}, consistent with natural rock mass transitions.

The choice of strength limits for the transition range – the lower-bound based on a review of cohesive soils, and the upper-bound ascribed to a strength limit considered valid for the material to completely behave as a rock, although reasonably well verified by the numerical modelling discussed in Carvalho et al., 2007, are still in need of additional field verification. Nevertheless the trends seem appropriate and effective, as illustrated by analysis of three fault zones from the Nathpa Jhakri headrace tunnel alignment (designated A, B and C on Figure 12), At each of these fault locations and at several other faults along the alignment (Hoek, 2001) quite wide gouge zones were encountered, comprising in the main granulated gneiss and/or mylonitized schist of such low strength that in several instances where high water pressures were also encountered significant mudflows occurred (Carter et al., 2005).
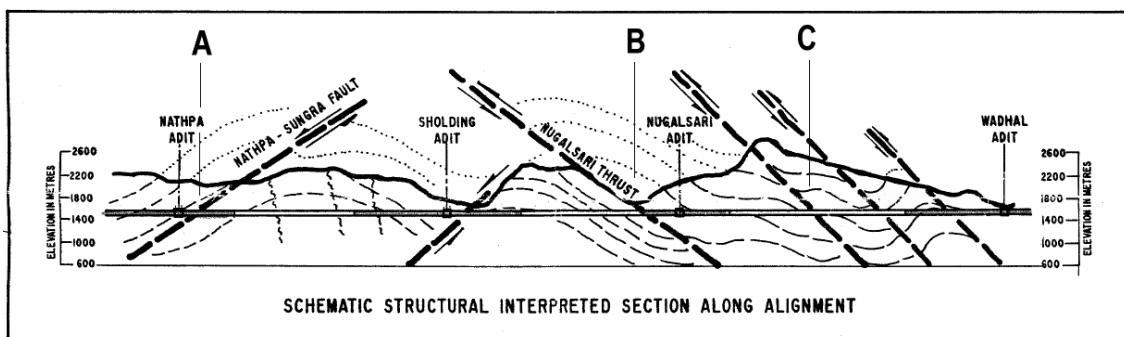

Figure 12: Location of Analyzed Fault Zones along Nathpa-Jhakri Headrace Tunnel

6.1 Characterization of the Fault Material

Although distinct differences were found in the character of each of the various major faults intersected in the tunnelling, in most cases a zone of soil-like gouge within margins of completely crushed rock was encountered. These gouge zones were often associated with or formed part of an alternating series of bands of good and bad rock consisting of schistose and granulated quartz-mica mylonite alternating with zones of more competent gneissic material. In all cases the wider gouge zones, which were of the order of 5-10m thickness, could be described as more soil-like than the gneissic rock-like material, that was often intensely foliated when not completely mylonitized.

6.1.1 Classical Hoek-Brown Parameters

Typical rock mass classification field assessment of one of these encountered fault zones, and checking against other Himalayan experience (Singh et al., 1992) using the NGI-Q-system descriptor codes, yielded the following parameter descriptions for the overall fault zone, based on typical margin zone conditions to the fault gouge shears:

$RQD = 20\%$ – for the margin zones to the gouge infills

$J_n = 20$ – crushed rock, earth-like

$J_r = 1$ – zone containing clay minerals, or crushed material

$J_a = 13$ – thick continuous zones or bands of clay

giving $Q' = \dfrac{20}{20} \times \dfrac{1}{13} = 0.0769$ = approximately equivalent to GSI=20

This rock quality estimate reflects overall mass conditions of the total fault fabric, not the specifics of just the cohesive gouge infills themselves, although such zones, in large part often dominate the strength behaviour of an entire fault. If considering just the gouge zones, intact "un-degraded" much higher RQD's might be applicable within the transition equations, but using a much lower UCSi value consistent with the gouge material itself. Here, however, for the purposes of modelling the entire fault behaviour (as discussed in the evaluations presented subsequently), a controlling strength of 5MPa along with typical values of m_i for schists in the range 7-10 have been ascribed. These values, which are considered reasonable mean estimates applicable for each overall fault zone, are based on the fact that core samples were largely unobtainable from the worst material in these faults and UCSi values of the order of 8.5 MPa were measured on mylonitized core from within fault margin zones away from the gouge sections. Based on these UCSi and m_i values, conventional Hoek-Brown m_b, s and a parameters of 0.402, 0.000138, and 0.54 were respectively estimated.

6.1.2 Transition Adjustment

Taking these conventional parameters and applying the transition function $f_T(\sigma_{ci})$ (eqn.1), with a UCS value of 5 MPa, assumed characteristic for the overall fault, we obtain:

$$f_T(\sigma_{ci}) = e^{\frac{-(UCSi - 5p_a)^2}{250 p_a}} = e^{\frac{-(5 - 0.5)^2}{25}} = 0.445$$

This suggests that intact properties should account for nearly 50% of the rock mass behaviour. Adjustment according to the transition function then results in the following modified H-B parameter values: $s^* = 0.445$; $a^* = 0.747$; $m_b^* = 2.691$

Comparing these modified values with the conventionally calculated H-B values the most significant change occurs in *s*, (viz *s* = 0.000138 by conventional calculation to *s**=0.445 through the transition relationship). As the *s* value provides the main control on strength under very low to no confinement, this change has a significant impact on the computed extent of the plastic zone. Pushing the envelope to linearization by taking *a** = 0.747 versus *a* = 0.544 and increasing m_b from 0.4 to m_b* = 2.7 results also in an increase in friction angle of about 15° at confinements greater than 2 MPa (ie., increasing ϕ from an unrealistically low 8° for the conventional Hoek-Brown envelope to a more probable 23° for the transition envelope).

6.2   Fault Modelling – Nathpa Fault

At the location of the Nathpa-Sungra fault, (Tunnel Station A on Figure 12) the cover is of the order of 650 m resulting in the following stress field (resolved in the plane of the analysis section): $\sigma_1 = 19.43\,MPa$; $\sigma_3 = 15.95\,MPa$; $\sigma_Z = 7.17\,MPa$; $\theta = 11.7°$,

where θ is the angle between σ_1 and the horizontal (x-axis).

As is evident from the excavation sequence shown in Figure 13 and the photographs and modelling results of the excavation stages illustrated in Figure 14, advance through this fault was difficult and extremely slow (in the order of 0.3m/day overall). As this tunnel was driven under Indian contract arrangements and NATM methods and equipment were not foreseen in the contract, excavation of the fault was carried out in a conventional 1940's style pilot heading layout with steel set supports rather than shotcrete shells, although NATM staged advance approaches were applied for both of the sidewall slash developments.
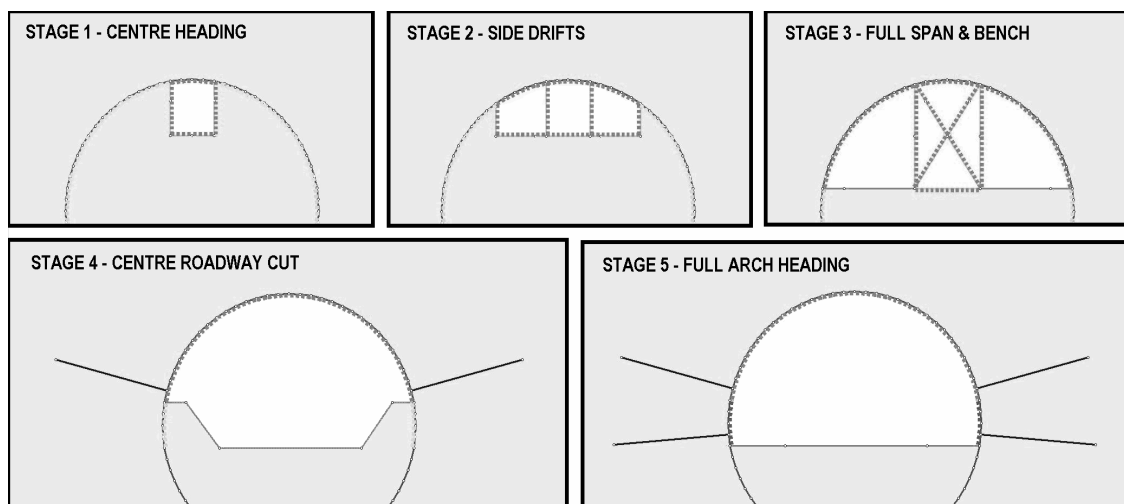
Figure 13: Excavation sequence through Nathpa fault

For the Nathpa Fault, excavation of the initial headings, although difficult, proceeded largely without incident until excavation of the central roadway cut, (Figures 13 & 14 – Stage 4) when large deformations began to be observed. In attempts to control the deformations and prevent the ribs from buckling and kicking-in, the feet of the main arch ribs were bolted back and in the worst zone of the fault the steel arch ribs were doubled up before slashing down the sidewalls and extending the feet to form the new arch profile, (Figures 13 and 14 – Stage 5).

This "sudden" onset of significant convergence is well replicated by the modelling results, which quite closely match with the convergence behaviour experienced during driving of the tunnel through the fault zone. As shown in the diagrams on the right side of Figure 14 the modelling matches well with field observations that deformation of the top heading was successfully contained by the support system until it had to be removed for the roadway deepening. At this stage, just prior to benching down for the roadway, even with the installed heavy set support in place, widening to full section and placing the central steel crib arrangement had resulted in crown displacements of about 30 cm while the side walls had converged by approximately 50 cm (Figure 14a).
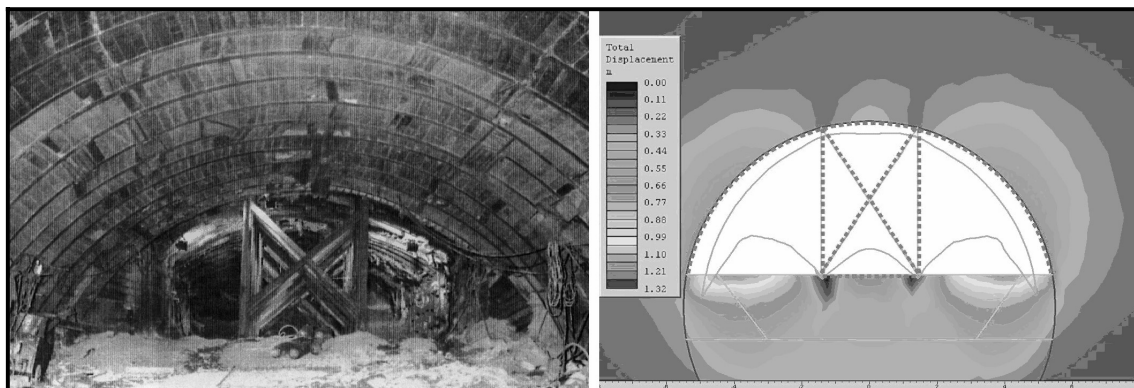
a) Supported top drift and crown slash – roof displacement ~ 30cm
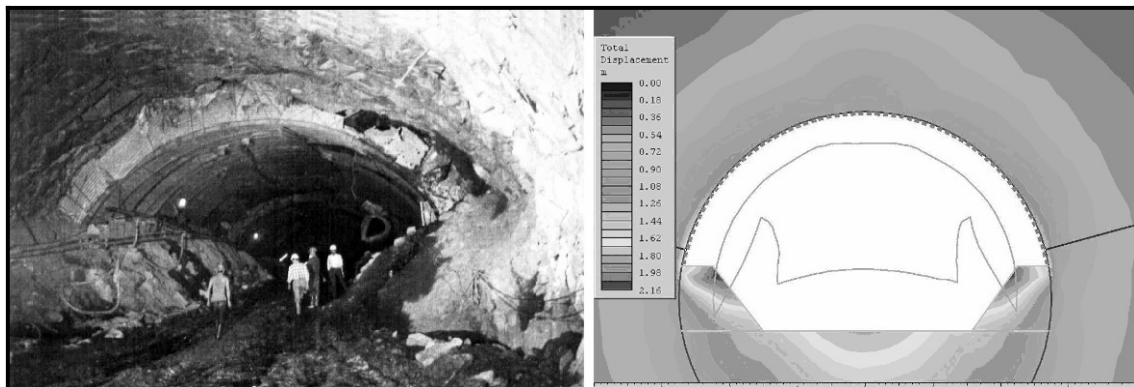
b) Removal of the crib and excavation of central roadway – radial displacement ~ 1 m

Figure 14: Comparison Results of Modelling of Nathpa Fault Zone behaviour using modified Hoek-Brown Transition $m*$, $s*$ and $a*$ parameters.

After removal of the support crib and excavating down to create the central roadway section, the crown and sidewalls further converged by about a metre (Figure 14b). What is also interesting and important is that after extending the double steel ribs to the current invert, the depth of the plastic zone above the crown is suggested by the modelling to have extended out to about 8m., a depth which is consistent with the roof caving experienced at the Nugalsari fault (Figures 15 and 16) in similar quality ground and also under about the same overburden cover depth (ref. Figure 12)

.

6.3   Nugalsari Fault

Excavation experience through the Nugalsari Fault Zone differed from that for the Nathpa Fault, as, at Nugalsari, due to the foliation dip and in particular the behaviour of the biotite schist a significant amount of geologically-controlled overbreak developed almost instantly on face exposure, as shown by the roof surveys in Figures 15 and 16.
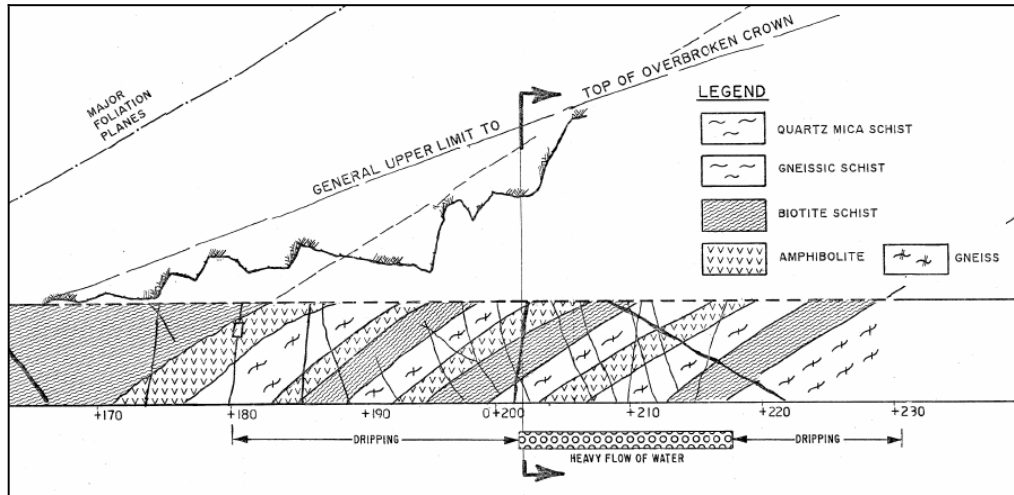

Figure 15: Longitudinal section through Nugalsari Fault (Location B on Figure 12), showing surveyed overbreak profile controlled by weak biotite schist gouge. (ref. Figure 16 for section)

Again the modelling of this fault zone using the low strength Hoek-Brown modified transition parameters *m**, *s** and *a** shows good replication with observed conditions, with the depth of the yielded plastic zone matching very closely the overbreak profile (even to the extent of the slight skew in damage due to stress obliquity (Figure 16).
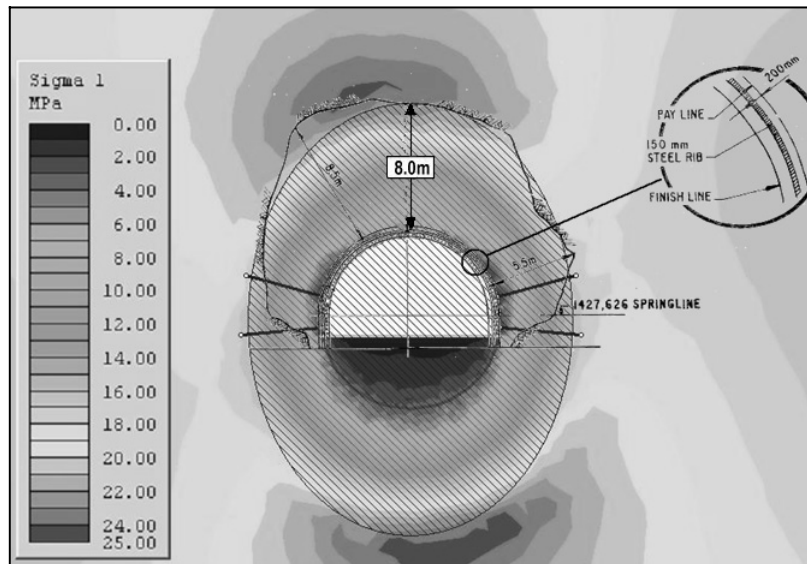

Figure 16: Major Principal Stress Contours and Plastic Zone computed with Phase2 based on Hoek-Brown Transition   *m*, s** and *a** parameters, as compared with actual surveyed overbreak profile at Station RD 0+202 (see Section location in Figure 15).

6.4 Wadhal Faulting

The last fault zone analyzed is one of a set of three sub-parallel major structures encountered in the Wadhal section of the headrace tunnel, all of which gave problems during excavation. The location of the particular fault chosen for analysis, which is sited at Tunnel Station C (as indicated on Figure 12) was encountered under the highest cover (of the order of 1000 m) resulting in the following stress field (resolved in the plane of the analysis section):

$$\sigma_1 = 24.46\,MPa; \quad \sigma_3 = 16.63\,MPa; \quad \sigma_Z = 10.06\,MPa; \quad \theta = 17°$$

where θ is again the angle between σ_1 and the horizontal (x-axis).

Again, as with the Nathpa Fault, excavation of all of the faults at Wadhal was carried out using an initial small top heading drift, fully supported with steel ribs with the sides then slashed and the crown ribs extended to the full tunnel springline geometry. This was again followed with a central bench cut to create a main roadway through the faulted section for access purposes prior to removing the sidewall abutment material supporting the feet of the crown arch ribs. Unfortunately, as benching to widen and deepen the tunnel to full section was underway in a segment of the tunnel approaching, but not directly within the fault margin, buckling and kick-in of a part of the main fault support system occurred, as illustrated in Figure 17. At the time it was presumed that this might well have resulted from stress readjustment ahead of the benching.

Figure 17: Predicted displacements before and after excavation of central bench

Modelling of this fault using the transition functions suggests not only that the plastic zone extended very deep into the crown (~ 14 m), but, as is evident from the two displacement plots on the right side of Figure 17, a major change in tunnel deformation behaviour is predicted to have occurred with final benching, with convergences increasing by 0.5m in the crown (from 1.15 m to 1.65 m) and with almost a metre of additional heave in the invert and sidewall abutment support zones, at the toe of the steel ribs (side walls). It is therefore not surprising that significant disruption occurred to the support system. It is also encouraging that with the use of the modified transition parameters *m**, *s** and *a**, very good modelling replication of actual failure behaviour is achieved.

7.0   CONCLUSIONS

Use of rockmass classification systems and the associated *m*, *s* and *a* parameter relationships linking GSI with the Hoek-Brown failure criterion provides a proven, effective and reliable approach for strength prediction for underground excavation design and support selection for most "normal" rockmasses:

  • with intact rock material strength, UCSi > 10–15MPa, and
  • with matrix yield behaviour dominated by shear mechanisms
     for ($m_i < 15$) for the full GSI range and
     for ($m_i > 15$) for GSI < 65.

Outside these limits, some discrepancies can arise between predicted and observed yield behaviour, which the use of the two transition relationships, previously proposed by Carter, Diederichs and Carvalho, 2007 are largely aimed to solve. The intended GSI and strength ranges for optimum applicability of these two transition relationships as compared with the generalized Hoek-Brown formulation are outlined in Table 2 below:
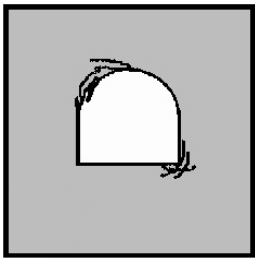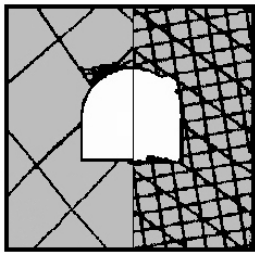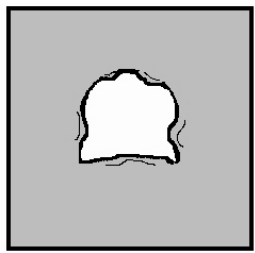
SPALLING CONDITIONS Massive, Essentially Unjointed Hard, Brittle Rock Masses $m_i > 15$ $GSI \cong 65$		$m_{SP} = s_{SP}\left(UCSi / |T|\right)$ $s_{SP} = \left(UCS*/UCSi\right)^{1/a_{SP}}$ $a_{SP} = 0.25$ *(peak)* & $= 0.75$ *(residual)* *and* $X_{TRANS} = X_{GSI} + (X_{GSI} - X_{SP})f_{SP}$ *where X_{SP} & $X_{GSI} = m_b$, s or a (for spalling or for classic H-B, respectively) and* $f_{SP} = \dfrac{1}{1+e^{100\left(2+\frac{D}{5}-\left(\frac{GSI}{60}\right)^{1/3}-\left(\frac{UCSi}{34T}\right)^{1/5}\right)}}$
NORMAL FRACTURED ROCKMASS CONDITIONS Classic Hoek-Brown & Classifications Applicable $m_i < 15$ – full GSI range $m_i > 15$ GSI<65		$\sigma_1 = \sigma_3 + UCSi\left(m_b\dfrac{\sigma_3}{UCSi} + s\right)^a$ $\dfrac{m_b}{m_i} = e^{\frac{GSI-100}{28-14D}}$; $s = e^{\frac{GSI-100}{9-3D}}$ $a = \dfrac{1}{2} + \dfrac{1}{6}\left(e^{\frac{-GSI}{15}} - e^{\frac{-20}{3}}\right)$
SQUEEZING CONDITIONS Matrix Dominated Equivalent Homogeneous Soil-like Rock Masses UCSi < 10–15MPa		$m_b^* = \left[m_b + (m_i - m_b)f_T(\sigma_{ci})\right]/(4a^* - 1)$ $s^* = s + (1-s)f_T(\sigma_{ci})$ $a^* = a + (1-a)f_T(\sigma_{ci})$ *where* $f_T(\sigma_{ci}) = \begin{cases} 1, & UCSi \le 0.5 MPa \\ e^{\frac{-(UCSi-0.5)^2}{25}}, & UCSi > 0.5 MPa \end{cases}$

Table 2: Modified Hoek-Brown Parameter Relationships for differing Rock Conditions, (where *UCSi* = Uniaxial compressive Strength; *T* = tensile strength; *UCS** = crack initiation threshold strength; *GSI* = geological strength index and f_{SP} and $f_T (\sigma_{ci})$ are the Spalling and Weak rock transition function relationships, and where m_i, m_b, *s*, *a* and *D* = Hoek-Brown generalized intact and rockmass friction and cohesion, exponent and damage parameters respectively).

Taken together, and used in combination with the original Hoek-Brown formulation for the "normal range of fractured rockmasses" it is hoped that use of these two proposed transition relationships will reliably extend the limits of applicability of GSI and the Hoek-Brown criterion for rockmass strength definition for rockmasses previously considered inappropriately handled by the Hoek-Brown relationships.

ACKNOWLEDGEMENTS

REFERENCES

Barton, N., Lien, R. and Lunde, J. (1974). *Engineering Classification of Rock Masses for the Design of Tunnel Support*, Rock Mechanics. Vol.6, pp.183-236.

Barton, N., Lien, R. and Lunde, J. (1977) *Estimating Support Requirements for Underground Excavations, in Design methods in Rock Mechanics*. Proc. 16ᵗʰ US Symp. On Rock Mechanics, Minneapolis, USA, pp.163-177.

Bieniawski, Z.T. (1973). *Engineering classification of rock masses*. Trans. S. African Inst. Civ. Engrs. 15(12): pp.335-344.

Bieniawski, Z.T. (1976). *Rock mass classification in rock engineering*. In Bieniawski (ed.), Proc. of the Symp. Exploration for Rock Engineering, 1: pp.97-106. Cape Town.

Carter, T.G., Steels, D., Dhillon, H.S. and Brophy, D., (2005). *Difficulties of Tunnelling under High Cover in Mountainous Regions*. Proc. Int. AFTES Congress, Tunnelling for a Sustainable Europe, Chambery, pp.349-358

Carter, T.G., Diederichs, M.S., & Carvalho, J.L. (2007) *A unified procedure for prediction of strength and post yield behaviour for rockmasses at the extreme ends of the integrated GSI and UCS rock competence scale*. Proc. 11th Congress of International Society for Rock Mechanics (ISRM), Lisbon, Portugal. pp.161-164

Carvalho, J.L., Carter, T.G. & Diederichs, M.S, (2007). *An approach for prediction of strength and post yield behaviour for rock masses of low intact strength*. Proc. 1st Can-US Rock Symp.. Meeting Society's Challenges & Demands. Vancouver. pp.249-257

Diederichs, M.S. (2003). *Rock fracture and collapse under low confinement conditions*. Rock Mechanics and Rock Engineering. 36 (5) pp.339-381

Diederichs, M.S. (2007). *Mechanistic Validation and Practical Application of Damage and Spalling Prediction Criteria for Deep Tunnelling*. The 2003 Canadian Geotechnical Colloquium. Canadian Geotechnical Journal. Vol.44 : 9 pp.1082-1116.

Diederichs, M.S, Carvalho, J.L., & Carter, T.G. (2007). *A modified approach for prediction of strength and post yield behaviour for high GSI rockmasses in strong, brittle ground.* Proc. 1st Can-US Rock Symposiium June, Vancouver. pp.277-28

Diederichs, M.S., Kaiser, P.K. & Eberhardt, E. (2004). *Damage initiation and propagation in hard rock tunnelling and the influence of near-face stress rotation.* Int. J. Rock Mech. & Min. Sci., 41: pp.785-812.

Griffith, A.A. (1921). *The phenomena of rupture and flow in solids.* Phil. Trans. Royal Soc. of London, 221A: pp.163-198.

Grimstad, E and Barton, N. (1993) *Updating the Q-System for NMT.* Proc. Int. Symp. On Sprayed Concrete, Fragernes.

Hoek, E. 1968. *Brittle failure of rock.* In Rock Mechanics in Engineering Practice. (Edited by Stagg and Zienkiewicz). London: Wiley and Sons. pp. 99-124.

Hoek, E., (2001) *Big Tunnels in Bad Rock*, Terzaghi Lecture, ASCE Journal of Gotechnical and Geoenvironmental Engineering, 127, No. 9, pp. 726-740

Hoek, E., Carranza-Torres, C.T, & Corkum, B.T. (2002). *Hoek-Brown failure criterion: 2002 edition.* In Hammah, Bawden, Curran & Telesnicki (eds.), Proc. of the 5th North American Rock Mech. Symp. Toronto, 7-10 July. University of Toronto Press. pp.267-274.

Kaiser, P.K., McCreath, D. and Tannant, D. (1995). *Canadian Rockburst Support Handbook.* Sudbury: Geomechanics Research Centre and CAMIRO.

Kumar, R and Dhawan, A. K., (1999). *Geotechnical Investigations of Nathpa Jhakri Hydro Electric Project* Proc. Workshop on Rock Mech. & Tunnelling, Shimla

Lajtai,E.Z. & Dzik,E.J. (1996). *Searching for the damage threshold in intact rock.* NARMS '96, Rotterdam: Balkema. pp.701-708.

Lee, S.M., Park, B.S., and Lee, S.W. (2004). *Analysis of rock-bursts that have occurred in a waterway tunnel in Korea.* Int. J. Rock Mech. & Min. Sci., 41(3). 6pgs.

Marinos, P. & Hoek, E. (2000). *GSI – A geologically friendly tool for rock mass strength estimation.* Proc. GeoEng2000 Conference, Melbourne: pp.1422-1442.

Martin, C.D. (1997). *The effect of cohesion loss and stress path on brittle rock strength.* Can. Geotech. J., 34 (5), pp.698-725.

Martin,C.D., Kaiser,P.K., & McCreath,D.R. (1999). *Hoek-Brown parameters for predicting the depth of brittle failure around tunnels.* Can. Geot. J., 36 (1): pp.136-151.

Palmström, A. (1995). *RMi a rock mass characterization system for rock engineering purposes.* Ph.D. Thesis, University of Oslo, 400pp.

Pelli, F., Kaiser, P.K., & Morgenstern, N.R. (1991). *Interpretation of ground movements recorded during construction of the Donkin-Morien tunnel.* Can.Geotech.Jour., 28(2): pp.239-254.

Pestman, B.J. & VanMunster, J.G. (1996). *An acoustic emission study of damage development and stress-memory effects in sandstone.* Int.J.Rock Mech.& Min.Sci. 33(6): pp.585-593

Potvin, Y., Hudyma, M. R. and Miller, H. D. S. (1989) *Design guidelines for open stope support.* CIM Bulletin 82(926).

Ryder, J.A. & Jager, A.J. (2002). *Rock Mechanics for Tabular Hard Rock Mines.* SIMRAC, Braamfontein.

Singh, B., Jethwa, J.L., Dube, A.K and Singh, B (1992) *Correlation between Observed Support Pressure and Rock Mass Quality.* J. Tunnelling and Underground Space Technology, Vol 7, #1, pp.59-74

Stacey, T.R. (1981). *A simple extension strain criterion for fracture of brittle rock*. Int. J. of Fracture, 18: pp.469-474.

Tapponier,P. & Brace,W.F. (1976). *Development of stress induced microcracks in Westerly granite*. Int. J. Rock Mech. & Min. Sci. and Geomech. Absrt., 13: pp.103-112.

Vemeer,P.A. & de Borst,R, (1984). *Non-associated plasticity for soils, concrete and rock*. Heron, 29. (3).

Wagner,H. (1987). *Design and support of underground excavations in highly stressed rock*. In Proc. 6th ISRM Congress, Montreal. Balkema, Rotterdam, 3: pp.1443-1457